



Title	Subpolar marginal seas fuel the North Pacific through the intermediate water at the termination of the global ocean circulation
Author(s)	Nishioka, Jun; Obata, Hajime; Ogawa, Hiroshi; Ono, Kazuya; Yamashita, Youhei; Lee, Keunjong; Takeda, Shigenobu; Yasuda, Ichiro
Citation	Proceedings of the National Academy of Sciences, 117(23), 12665-12673 https://doi.org/10.1073/pnas.2000658117
Issue Date	2020-05-27
Doc URL	http://hdl.handle.net/2115/79850
Type	article (author version)
File Information	Proceedings of the National Academy of Sciences of the United States of America2000658117.pdf



[Instructions for use](#)

1 **Sub-polar marginal seas fuel the North Pacific through the intermediate water at**
2 **the termination of the global ocean circulation**

3
4 Jun Nishioka^{a,b*}, Hajime Obata^c, Hiroshi Ogawa^c, Kazuya Ono^a, Youhei Yamashita^d,
5 Keun Jong Lee^c, Shigenobu Takeda^e and Ichiro Yasuda^c

6
7 ^a*Pan-Okhotsk Research Center, Institute of Low Temperature Science, Hokkaido University,*
8 *Sapporo, Japan*

9 ^b*Arctic Research Center, Hokkaido University*

10 ^c*Atmosphere and Ocean Research Institute, The University of Tokyo, Kashiwa, Japan*

11 ^d*Faculty of Environmental and Earth Science, Hokkaido University, Sapporo, Japan*

12 ^e*Graduate School of Fisheries and Environmental Sciences, Nagasaki University, Nagasaki*
13 *Japan*

14
15 ***Corresponding author**

16 Jun Nishioka: +81-11-706-7655, nishioka@lowtem.hokudai.ac.jp

17 ORCID-ID: 0000-0003-1723-9344

18
19 Other authors ORCID-IDs

20 Hajime Obata: 0000-0002-5289-1592,

21 Hiroshi Ogawa: 0000-0002-4920-8668

22 Youhei Yamashita: 0000-0002-9415-8743

23 Shigenobu Takeda: 0000-0002-4997-1583

24 Ichiro Yasuda: 0000-0002-4742-6880

25
26 **Classification**

27 Physical Sciences; Earth, Atmospheric, and Planetary Sciences

28
29 **Keywords:** Macro nutrients, Dissolved iron, The North Pacific Ocean, Island chains,
30 Mixing, End of conveyor belt, GEOTRACES

31
32
33 **Author Contributions**

34 J.N., H.Ob, and I.Y. contributed to the design of the research. J.N., H.Ob., H.Og. and
35 I.Y. contributed to managing the research cruises. J.N. performed all iron analyses, J.N.
36 and H.Og. performed nutrient analysis, and K.O. was responsible for other onboard

37 measurements. I.Y. and K.L. measured turbulent mixing parameters in this study. J.N
38 analysed the results and prepared the manuscript with inputs from H.Ob., H.Og., Y.Y.
39 S.T. and I.Y..

40

41 **This paper includes:**

42 The manuscript, references, methods, figures, and supporting information (figures and
43 tables). We include the 5 main manuscript figures, 8 supporting figures and 2
44 supporting tables individually.

45

46 **Abstract**

47 **The mechanism by which nutrients in the deep ocean are uplifted to maintain**
48 **nutrient-rich surface waters in the subarctic Pacific has not been properly**
49 **described. The iron (Fe) supply processes that control biological production in the**
50 **nutrient-rich waters are also still under debate. Here, we report the processes that**
51 **determine the chemical properties of intermediate water and the uplift of Fe and**
52 **nutrients to the main thermocline, which eventually maintains surface biological**
53 **productivity. Extremely nutrient-rich water is pooled in intermediate water (26.8–**
54 **27.6 σ_θ) in the western subarctic area, especially in the Bering Sea basin. Increases**
55 **of two to four orders in the upward turbulent fluxes of nutrients were observed**
56 **around the marginal sea island chains, indicating that nutrients are uplifted to the**
57 **surface and are returned to the subarctic intermediate nutrient pool as sinking**
58 **particles through the biological production and microbial degradation of organic**
59 **substances. This nutrient circulation coupled with the dissolved Fe in**
60 **upper-intermediate water (26.6–27.0 σ_θ) derived from the Okhotsk Sea evidently**
61 **constructs an area where has one of the largest biological CO₂ drawdown in the**
62 **world ocean. These results highlight the pivotal roles of the marginal seas and the**
63 **formation of intermediate water at the end of the ocean conveyor belt.**

64

65 **Significance Statement**

66 A correct understanding of the iron and macro-nutrient dynamics at the termination of
67 the global ocean conveyor belt circulation is critical for understanding the global carbon
68 cycle and its changes in geological time scale. Newly obtained and compiled data sets
69 of iron and macro-nutrients with the vertical mixing magnitude in the subarctic Pacific
70 and marginal seas indicate the processes that determine the nutritional status of
71 intermediate waters and the mechanisms by which sub-polar marginal seas fuel the
72 North Pacific Ocean through the intermediate water. The intermediate water formation
73 processes play a major role in the connection of nutrients between the deep water and
74 the surface water above it, and sustain biological production, at the termination of the
75 global nutrient circulation.
76

77 Although the subarctic Pacific is a high nutrient low chlorophyll region (HNLC),
78 where high concentrations of macro-nutrients (hereafter “nutrients”) remain in the
79 surface and phytoplankton growth is limited by iron (Fe) availability (1–3), this area has
80 the largest biological CO₂ drawdown among the world oceans (4), and the high
81 productivity of the region’s ecosystem and fisheries (5) must be sustained by supplies of
82 both Fe and nutrients into the euphotic zone.

83 Since the sinking of biogenic particles exports nutrients towards the
84 intermediate/deep sea, the maintenance of surface nutrients requires a return path of the
85 nutrients from the deep ocean (6). In the Southern Ocean, the main nutrient return path
86 from deep water by upwelling and subsequent entrainment into sub-Antarctic mode
87 water has been well explained (6). In the North Pacific high latitude region, nutrients
88 accumulate in deep water with old ¹⁴C age (7–9). In previous ¹⁴C observations in the
89 North Pacific, the oldest water was clearly observed at approximately 2000–2500 m
90 depth, and the deep water returned southward below the intermediate water (7, 10),
91 which had the highest nitrate and phosphate concentrations, indicating that the high
92 nutrient deep water does not directly affect the surface layer in the subarctic Pacific.
93 Although previous studies imply that the nutrient return path to the surface exists in the
94 northwest corner of the Pacific (6, 11), detailed mechanisms by which nutrients return
95 to the surface layer and how HNLC water is formed in the North Pacific have not been
96 described.

97 In addition to winter entrainment mixing, an important factor in understanding the
98 return of nutrients to surface water is vertical turbulent diapycnal mixing. Because
99 density stratification in the ocean generally prevents vertical transport (12), it is difficult

100 for dense nutrient-rich deep water and shallow less-dense nutrient-depleted water to be
101 exchanged. Therefore, vertical turbulent mixing is crucial for the quantitative evaluation
102 of the return of nutrients from the deep layer to the surface. An important factor for
103 controlling biological production in the nutrient-rich region is the formation of chemical
104 properties of intermediate water (6), including nutrients and the limiting micro-nutrient
105 “Fe”. North Pacific Intermediate Water (NPIW) is formed under the strong influence of
106 the marginal seas (13–15) and may play a major role in the connection of nutrients
107 between the deep water and the surface water above it (6). Furthermore, additional to
108 atmospheric-dust deposition, recent trace metal measurements have highlighted the
109 importance of localized sources of external Fe, such as river discharge, shelf sediment
110 load, hydrothermal input and sea ice melting (16-21). In the North Pacific, loading Fe
111 from the continental margin and shelves of the marginal seas, from which Fe is
112 transported by intermediate water circulations, are highlighted in recent studies (11,
113 22-26). There are still debates about the quantitative contributions of atmospheric dust
114 Fe and oceanic Fe transport processes to Fe supply processes in the North Pacific (19,
115 27–29). To quantitatively elucidate the supply processes of Fe and nutrients to the
116 surface in the North Pacific, it is necessary to comprehensively understand formation of
117 the chemical properties of basin-scale intermediate water, as well as the mixing and
118 circulation in this area (20).

119 In this study, we compiled comprehensive observed data of chemical water
120 properties (Table S1, which is including newly obtained high quality data from GP02 of
121 GEOTRACES section line, the western Bering Sea, the Aleutian island chains (ICs) and
122 the East Kamchatka Current (EKC)), including dissolved Fe (dFe) and nutrients, with

123 physical parameters of vertical mixing, in the North Pacific including the marginal seas
124 and areas around the Kuril and the Aleutian ICs (Fig. 1a, see Methods). This dataset can
125 be used to analyse the distribution of the chemical parameters of isopycnal surfaces, and
126 we succeed in showing the overall spatial distribution and circulation of Fe and
127 nutrients in the North Pacific for the first time.

128 **Spread of Fe from the Okhotsk Sea via ventilation**

129 We first constructed a diagram showing the 3D distribution of dFe in the North
130 Pacific, including its subpolar marginal seas (the Okhotsk Sea and the Bering Sea) (Fig.
131 1b). From this dataset, we inferred the characteristics of dFe circulation in the North
132 Pacific. The dFe concentration in surface waters is low throughout the subarctic Pacific
133 region, except for in the shelf areas of the Okhotsk Sea and the Bering Sea (Fig. 1c).
134 The vertical section profile of dFe along GP02 (in Fig. 1b, See SI Appendix, Fig. S1f)
135 was updated to cover the full section from the western to the eastern subarctic Pacific in
136 this study. The eastern side of the subarctic Pacific has a continental shelf source of dFe
137 along the Alaskan Stream (AS) (Fig. 1b, See SI Appendix, Fig. S1f), as previously
138 reported (22). This high-dFe water of the AS is basically confined to the nearshore area,
139 because the boundary current (AS) passes along the coast, although eddy transports of
140 the high-dFe water to offshore occasionally occur (30). The sections also clearly
141 indicate that dFe concentrations are highest in the intermediate water on the western
142 side of the subarctic Pacific (Fig. 1b, See SI Appendix, Fig. S1f) as previous studies
143 suggested (11, 24, 25).

144 The horizontal distribution indicated by isopycnal analysis in this study clearly
145 shows evidence that the high dFe source in the intermediate waters in the western
146 subarctic Pacific is the marginal seas. The upper (U-) NPIW density range (26.6–27.0 σ_θ ,
147 where 26.8 σ_θ is the median density of U-NPIW) is strongly influenced by the Okhotsk
148 Sea Intermediate Water (OSIW), whereas the lower (L-) NPIW density range (27.0–
149 27.5 σ_θ) is influenced mainly by the EKC and the Western Subarctic Gyre (WSG) (13).
150 The isopycnal analysis clearly indicates that the dFe-rich water in the U-NPIW density
151 range (Fig. 1d), in which dissolved oxygen (DO) is also higher than surrounding water
152 (Fig. 2a), is derived from the OSIW that originates in the Okhotsk Sea shelf and
153 propagates along the 26.8 σ_θ isopycnal surface to the western North Pacific (mainly
154 west of 155°E) (Fig. 1d). In contrast, in the L-NPIW density range, e.g., at 27.5 σ_θ (Fig.
155 1e), dFe is high across a wide area in the western subarctic Pacific, particularly along
156 the northern part of the WSG including the areas southeast of the Kamchatka Peninsula,
157 the western Bering Sea basin and around the eastern Aleutian Islands (hereafter we
158 define the region as “the northern WSG”) (Fig. 1e). The dFe distribution in the Oyashio
159 region can be explained by the direct influence of both waters transported from the
160 Okhotsk Sea to U-intermediate water and the EKC influence on L-intermediate water
161 (See SI Appendix, Fig. S2a-f).

162 **Formation of subarctic intermediate water nutrient pool**

163 Intermediate water, which is extremely rich in phosphate (PO_4) but low in DO,
164 was observed on the 26.8 σ_θ isopycnal surface in the northern WSG (Fig. 2a and 2b),
165 especially in the western Bering Sea basin, in the southeast of the Kamchatka Peninsula
166 (Fig. 2a and 2b, See SI Appendix, Fig. S1a and S1b) and around the eastern Aleutian

167 Islands (Fig. 2a and 2b). In fact, the water was observed in the wide density range of
168 $26.6\text{--}27.6 \sigma_\theta$ (which covers both density ranges of U- and L-intermediate water) along
169 GP02 in the entire subarctic area (See SI Appendix, Fig. S1d and S1e). In addition, the
170 calculated percentage of regenerated (reg-) PO_4 out of the total PO_4
171 $((\text{AOU} \times R_{\text{P:DO}}) / \text{observed } \text{PO}_4 \times 100, \text{ see Method})$ in a section along the EKC line
172 indicates that more than half the total PO_4 in the density range of $26.8\text{--}27.6 \sigma_\theta$ is
173 reg- PO_4 (Fig. 2c). The intermediate water with high proportion of the reg- PO_4 is also
174 observed in the same density range in the subarctic west to east section along the GP02
175 line (Fig. 2d), indicating that the reg- PO_4 -rich intermediate water is widely propagated
176 not only in the northern WSG but also eastward to the Alaskan Gyre (Fig. 2d, See SI
177 Appendix, Fig. S1d and S1e). That is, high nutrients are pooled in the subarctic
178 intermediate water ($26.8\text{--}27.6 \sigma_\theta$, this is greater depth than previous definition of NPIW
179 density range $27.5 \sigma_\theta$ (13)) in the northern WSG and Alaskan Gyre; we henceforth call
180 the water the “subarctic intermediate nutrient pool (SINP)”. Above the SINP, surface
181 productive areas were observed by satellite chlorophyll images in the margin of the
182 northern WSG along the regions of the Oyashio, southeast of the Kamchatka Peninsula,
183 around the Kuril and the Aleutian ICs and the Bering Sea shelf slope (See SI Appendix,
184 Fig. S3). The formation of the chemical properties of the SINP can only be explained by
185 the consumption of DO and regeneration of PO_4 , as particulate organic matter that sinks
186 from the surface productive areas decomposes during the intermediate water circulation
187 in the subarctic Pacific and its marginal seas. In contrast, the SINP formation cannot be
188 explained by the direct transport of the nutrient-rich deep water because the deep water
189 has a higher DO concentration.

190 In the U-NPIW density range, where the influence of Okhotsk Sea water is strong,
191 a meridional vertical cross section of the low percentage of reg-PO₄ along Okh-155 in
192 the Okhotsk Sea to along 155°E in the North Pacific (Fig. 2e) clearly indicates that
193 newly formed (ventilated) water in the Okhotsk Sea which has relatively low PO₄ and
194 high DO (Fig. 2a and 2b) is distributed in the U-NPIW density range, and the U-NPIW
195 circulation mainly transports the preformed (pre-) PO₄ onto the SINP.

196 **Main nutrient return path from the intermediate to the surface**

197 Our data set is mostly collected in summer season. In the dataset, the horizontal
198 distribution of nitrate + nitrite (N) concentrations near the surface (Fig. 3a) are variable,
199 with concentration maxima observed around the Kuril and the Aleutian ICs, whereas the
200 N concentrations at depth on the 26.8 σ_θ surface (Fig. 3b) (in the SINP waters) at the
201 northern WSG are uniformly high. The surface water maxima (Fig. 3a) suggest that
202 upwelling occurs around the ICs. Near these ICs, vertical turbulent fluxes of N from
203 intermediate to surface waters, determined by direct measurements of turbulent vertical
204 diffusivity (using average 100-500 m, see Methods), are two to four orders of
205 magnitude greater than those in the open ocean (Fig. 3c, See SI Appendix, Table S2).
206 The fluxes are largest in the Kuril Straits (average daily N flux, ~100 mmol/m²/day) and
207 second largest in the Aleutian passes (average daily N flux, ~10 mmol/m²/day), and in
208 both these regions, they are much greater than the fluxes in the subarctic Pacific
209 (average daily N flux, ~1 mmol/m²/day) (Fig. 3c, See SI Appendix, Table S2). These
210 results indicate that the Kuril and Aleutian ICs are the hot spots that return nutrients
211 from the intermediate water to the surface water through the enhanced turbulent
212 diapycnal mixing caused by interactions of tidal currents with the rough topography

213 (31-33). Accounting for the IC areas where turbulent mixing occurs, the estimated
214 uplifted annual N fluxes around the Aleutian and the Kuril ICs ($10^{11} \sim 10^{13} \text{ mol y}^{-1}$,
215 geometric mean $\sim 10^{12} \text{ mol y}^{-1}$ (See SI Appendix, Fig. S8)) can account for less than
216 10 % of N pooled in the SINP ($4.2 \pm 0.4 \times 10^{14} \text{ mol}$) per year and comparable to the
217 exported N from surface to below the winter mixed layer in the whole northern
218 subarctic Pacific ($\sim 10^{12} \text{ mol y}^{-1}$) (34-35) (See SI Appendix, Fig. S4), whereas the
219 estimated flux of uplifted N only by the turbulent mixing in the open ocean in the
220 subarctic Pacific ($\sim 10^{11} \text{ mol y}^{-1}$; the values estimated by data obtained from KNOT,
221 CL2-CL16, See SI Appendix, Fig. S7) is one order of magnitude smaller than the
222 amount of exported N in this region. The geometric mean of total uplifted annual N flux
223 estimated in this study is $\sim 10^{12} \text{ mol y}^{-1}$ (See SI Appendix, Fig. S8). The value, however,
224 might be underestimated or there is another missing upward flux of N (or exported N
225 might be overestimated) because the uplifted N flux must be greater than the exported N
226 for maintaining high nutrient surface water in the subarctic Pacific. Together with
227 previously reported information (36), approximately $< 1\%$ of N in the SINP is annually
228 transported to NPIW. Additionally, considering the nutrient data with dFe data set
229 analysis, the chemical properties of uplifted intermediate waters around the Aleutian ICs
230 have a lower dFe:N ratio than the diatom demand (see next section). These results
231 indicate that this enhanced mixing around the Aleutian ICs, combined with winter
232 surface mixing, plays an important role in the supply of nutrient-rich (but biologically
233 Fe limited) waters from the SINP to the surface and in maintaining HNLC waters in the
234 surface layer of the subarctic Pacific and the western Bering Sea basin (see next
235 section).

236 There must be another important role of mixing around the ICs. To balance the
237 nutrient budget in the SINP, the interaction between the deep water and the intermediate
238 water is necessary. Nutrients need to be supplied from the deep water to the SINP by the
239 turbulent mixing processes around the ICs (Fig. 4a, 4b) by the amounts that are laterally
240 transported by the NPIW to low latitudes from the SINP (Fig. 4c, See SI Appendix, Fig.
241 S5). Understanding the nutrient transport interactions between the deep water and the
242 intermediate water will be an issue for the future, and it is necessary to measure
243 turbulence in the abyssal zone.

244 **Intermediate water controls biological productivity**

245 The intermediate water chemical properties are crucial for the productivity of the
246 North Pacific. The nutrient circulation in the SINP coupled with the dFe in
247 U-intermediate water derived from the Okhotsk Sea (external Fe input) (Fig. 1b, Fig. 1d,
248 Fig. 4b) leads to a relatively high dFe:N ratio in the intermediate waters. The dFe:N
249 ratios are higher in the Okhotsk Sea and around the Kuril ICs in the subsurface to
250 intermediate density ranges (Fig. 5a, 5b, 5c) than that around the Aleutian ICs and in the
251 Bering Sea basin (Fig. 5f), indicating that the Fe-rich water diapycnally upwells to the
252 surface around the Kuril ICs by strong turbulent mixing (Fig. 5a, 5b, 5c). The water,
253 which has a high dFe:N ratio, spreads downstream along the Oyashio; the ratio remains
254 high west of 155°E along the U-intermediate water pathway (Fig. 5a and 5d), while the
255 ratio decreases rapidly east of 155°E (Fig. 5a and 5e), probably because of mixing with
256 low-Fe water and scavenging during water transport. In the western subarctic and the
257 Oyashio–Kuroshio transition zone, the upper rim of U-NPIW (isopycnal surface 26.6
258 σ_θ), which also has a relatively high dFe:N ratio (Fig. 5a), is able to influence the

259 surface water because the shallower isopycnal surfaces at $26.6 \sigma_{\theta}$ (~120 m) in the
260 western subarctic Pacific outcrop to the surface in wintertime (Fig. 5d and 5g) (15, 37).
261 The area where these waters with the high dFe:N ratio outcrop corresponds to the area
262 where greater nutrient and biological pCO_2 drawdown occur (4, 38). Although the Fe
263 supply is not high enough to prevent Fe limitation (11), which causes persistent HNLC
264 in the subarctic Pacific including around the ICs (39) and the western Bering Sea Basin,
265 Fe supplied from the intermediate water stimulates diatom blooms in the western
266 subarctic and the Oyashio-Kuroshio transition zone (40).

267 Our results clearly indicate that, in the subarctic Pacific, where high nutrients are
268 distributed (41) at the end of global nutrient circulation (7), sub-polar marginal seas and
269 intermediate waters play pivotal roles for linking deep water to surface biogeochemistry
270 and leading an area with among the highest nutrient concentration in the surface water
271 (41) and the largest biological pCO_2 drawdown area in the world ocean (4). We showed
272 the processes determining the chemical properties of intermediate waters (including
273 NPIW), and the mechanisms that determine how intermediate waters affect the supply
274 of Fe and nutrients to the main thermocline and maintain surface productivity. The
275 chemical properties of NPIW likely have a strong influence on biological productivity
276 not only at high latitudes but also at low latitudes in subtropical area due to nutrient and
277 Fe entrainment in the North Pacific (6). The sub-polar marginal seas are changing under
278 the influence of climate change, with changes such as the weakening of ventilation and
279 intermediate water circulation with decreasing sea ice formation (42). Therefore, our
280 findings have important implications for predicting the impact of climate change on the
281 global nutricline, biological productivity and the carbon cycle.

283 **Methods**

284 **Field observations.**

285 Comprehensive observations for investigating Fe in the North Pacific were carried
286 out from 1998 to 2018. Vertical profiles of dissolved Fe concentrations were collected
287 in 24 cruises, which included marginal seas. All cruises that observed the dFe data are
288 listed in Table S1. Seawater from the surface to bottom layers was collected with
289 acid-cleaned Teflon-coated 10 or 12 L Niskin-X bottles that were mounted on a CTD
290 (SBE 9 plus) with a carousel multi-sampling system (SBE32) during all cruises in this
291 study. The details of the sampling methods used for each cruise have been described
292 elsewhere (11, 24, 25, 26, 40, 44, 45).

294 **Dissolved Fe measurements**

295 To sub-sample from the Niskin-X sampler during the R/V *Hakuho Maru* cruise, the
296 samplers were transported in a clean air bubble (filled with air that had been passed
297 through a high-efficiency particulate air filter). To sub-sample from the Niskin-X
298 sampler during the R/V *Professor Multanovskiy*, *Professor Kromov* cruise, the samplers
299 were placed in a clean tent. A 0.22 µm Millipak filter (Millipore co.) or a 0.2 µm
300 Acropak filter (Pall Co.) was connected to the Niskin-X spigot; then, the filtrate was
301 collected in acid-cleaned 125-mL low density polyethylene (LDPE) bottles (Nalgene
302 Co., Ltd). We confirmed that there were no significant differences between the dFe
303 concentrations measured using the Acropak filter and the Millipak filter (See SI
304 Appendix, Fig. S6b).

305 Before 2006, the filtrate (<0.22 µm and 0.2 µm) was directly adjusted to pH 3.2
306 with a formic acid (10 M)–ammonium (2.4 M) buffer. After 2006, the filtrate (<0.22 µm
307 and 0.2 µm) was adjusted to pH < 2 by the addition of ultrapure HCl (Tamapure
308 AA-10) and then allowed to remain at least for 24 h to three months at room
309 temperature in the onboard clean room. Each sample was then adjusted to pH 3.2 just
310 before measurements by the addition of an ammonium solution and a formic acid (10
311 M)–ammonium (2.4 M) buffer. Then, dFe, defined as the leachable Fe in the filtrate at
312 pH < 2, was analysed in the onboard or onshore laboratory using a flow-injection
313 analysis (FIA) chemiluminescence detection system (46). All sample treatments were
314 performed under laminar flow in the onboard or onshore clean-air laboratory. We
315 confirmed that there were no significant differences between these two different
316 acidified methods for open ocean sample (See SI Appendix, Fig. S6a).

317 The quality of dFe measurements was controlled by measuring house standard
318 seawater. Additionally, the dFe measurements and reference seawater analyses in this

319 study after 2006 were quality-controlled using SAFe (Sampling and Analysis of Iron)
320 cruise (47) reference standard seawater (obtained from the University of California
321 Santa Cruz for an inter-comparison study). We measured a SAFe reference sample
322 during every sample measurement run of the FIA instrument performed in the onboard
323 and onshore laboratories in the cruise for the GEOTRACES program (Table S1). The
324 consensus values for Fe(III) in the SAFe reference standard seawater are 0.093 ± 0.008
325 nM (S) and 0.933 ± 0.023 nM (D2) (May 2013, www.geotraces.org), and, in
326 GEOTRACES official cruise, for instance, we obtained values of 0.098 ± 0.010 nM (n
327 = 12) (S) and 0.976 ± 0.101 nM ($n = 10$) (D2) using our method. This good agreement
328 demonstrates that our data quality was high and that our data are comparable with the
329 global GEOTRACES dataset. The detection limit (three times the standard deviation of
330 the Fe(III) concentration (0.036 nM) of purified seawater that had been passed through
331 an 8-quinolinol resin column three times to remove Fe) was 0.020 nM. See ref. (11, 24,
332 25, 26, 40, 44, 45).

333

334 **Nutrient measurements**

335 Nutrient (nitrate + nitrite, phosphate, silicate) concentrations were also analyzed
336 in water samples collected from the same stations. Nitrate + nitrite (define as N in this
337 study) concentrations were measured using a BRAN-LUEBBE auto-analyser (TRACCS
338 800), and a BL-Tec auto-analyser (QuAAtro). Most of the nutrient measurements in this
339 study were quality-controlled using KANSO reference material (KANSO Co.). In this
340 study, we also refer nutrient data from JAMSTEC MR04-04 cruise
341 (<http://www.godac.jamstec.go.jp/darwin/cruise/mirai/mr04-04/j>)

342

343 **Other parameters**

344 Salinity and temperature were measured using a conductivity-temperature-depth
345 (CTD) sensor, and dissolved oxygen (DO) concentrations were measured using an
346 oxygen sensor connected to a CTD. The DO concentration was also measured on board
347 by the Winkler titration method, and the DO concentration obtained by the sensor was
348 calibrated using the concentration determined by the Winkler method. The oxygen
349 solubility was calculated and apparent oxygen utilization (AOU) was then calculated as
350 the difference between the solubility and the measured DO concentration.

351

352 **Calculation for percentage of regenerated (reg-) PO₄**

353 The percentage of regenerated (reg-) PO₄ in total PO₄ was calculated by the
354 equation “(AOU×R_{P:DO})/observed PO₄×100”. In this equation, R_{P:DO} is a regenerated
355 mol ratio for phosphate to oxygen; we employed a R_{P:DO} of 170 from reference (48).
356

357 **Estimating vertical fluxes of dFe and nitrate**

358 The material flux was estimated at the Kuil and the Aleutian ICs. We employed a
359 simple calculation to estimate the vertical flux of dFe and N from the subsurface to
360 the surface at the ICs using the following equations.
361

$$362 \quad \text{dFe Flux} = K_{\rho} \times (\text{dFe}/\text{dz}), \quad \text{N Flux} = K_{\rho} \times (\text{dN}/\text{dz})$$

363
364 Our measured dFe and N vertical profiles at the ICs strait were already influenced by
365 the strong mixing, and the gradients (dFe/dz and dN/dz) in the profiles from surface to
366 subsurface were disrupted. Thus, the gradients in the profiles at the IC strait were not
367 suitable for estimating the material flux from intermediate water to surface water. To
368 evaluate the flux from the intermediate water to the surface water at the IC straits, we
369 used the vertical profile of dFe and N obtained around the straits (locations are blue dots
370 in See SI Appendix, Fig. S7), which we used to approximate the profiles before the
371 water was influenced by the mixing process. The surface to subsurface gradients of dFe
372 (dFe/dz) and N (dN/dz) were evaluated at all stations located around the straits (blue
373 dots for the ICs and yellow dots for the subarctic Pacific). To estimate fluxes, we
374 combined the gradients with the measured snapshot of vertical diffusivity K_{ρ} ($=0.2\varepsilon N^2$
375 where ε is turbulent kinetic energy dissipation rate in W/kg and $N^2 = -g\rho_z/\rho$ where N^2 is
376 squared buoyancy frequency, where g and ρ are the gravitational acceleration and
377 reference potential density, respectively) for depths of 100-500 m. The K_{ρ} was
378 measured by using a free-fall vertical microstructure profiler (VMP2000 Rockland
379 Scientific International co.) (31, 32, 33) on the cruise Kh06, Kh07, KH-09-4 for the ICs
380 waters and on the cruise KH-08-2 for the open waters in the western subarctic Pacific
381 (See Table S2). The K_{ρ} was also measured by using CTD-attached fast-response
382 thermistors (AFPO7, Rockland Scientific International co.) (49, 50) on the KH-17-3
383 cruise for open water in the subarctic Pacific (See Table S2). Comparison study between
384 these two measurement methods have been conducted at 100 stations in several cruises
385 (50), including KH-09-4 (See Table S2) (50). Turbulence intensity estimated from
386 CTD-fast-response thermistors was compared to those by free-fall microstructure
387 profilers, conducted at the same location within 2h, and the result was reported in Goto
388 et al. (2018) (50) where ε is valid for $10^{-10} < \varepsilon < 10^{-8}$ W/kg after response correction (49)

389 and data screening (50), and it has been confirmed that ϵ from both measurement
390 methods are comparable and within a factor of 3 (50).

391

392 **Estimated budget of nitrate+nitrite (N) among the surface, intermediate, and** 393 **deep waters** (See SI Appendix, Fig. S4, Fig. S8).

394 The annual transport of N from the SINP to the surface was calculated by the geometric
395 mean of uplifted N fluxes at the Kuril and Aleutian ICs accounting for the approximate
396 area where mixing occurs (the Kuril ICs: $1.12469E+11$ m² and Aleutian ICs:
397 $2.14087E+11$ m², the IC areas were defined to cover where the depth-integrated tidal
398 energy dissipation rate estimated from a global barotropic tide model (51) were higher
399 than 5.0×10^{-2} W/m² along the ICs) (See SI Appendix, Fig. S8). The uplifted N flux in
400 the open ocean in the subarctic Pacific was calculated by the geometric mean fluxes in
401 the subarctic Pacific, accounting for the area of the northern WSG ($4.92255E+12$ m²)
402 and Alaskan Gyre ($3.02873E+12$ m²). Exported N from the surface through the winter
403 mixed layer depth was calculated by using number of $1.49 \sim 2.3$ mol-C m⁻² y⁻¹, which
404 was previously reported in the WSG (34, 35) and the Alaskan Gyre (35), accounting for
405 the area of the northern WSG and Alaskan Gyre (See SI Appendix, Fig. S8). N pooled
406 in the SINP was calculated with an average N concentrations (42 ± 2.3 μ mol/kg) in the
407 intermediate water range between 26.8-27.6 at the stations, the thickness of the
408 intermediate water (1237 ± 137 m), in the whole subarctic Pacific and the western
409 Bering sea, and the area of the northern WSG and Alaskan Gyre (See SI Appendix, Fig.
410 S8).

411

412 **Ocean Data View parameters.**

413 Ocean Data View (ODV; <http://odv.awi.de/>) (52) was used to calculate and produce
414 plots for the basin-scale isopycnal surface distribution and vertical section profiles of
415 each parameter in Figs. 1, 2, 3, 5, Fig. S1, S2, S5, S7.

416

417 **Data availability.**

418 The data that support the findings of this study are available at the site of following
419 URL. <https://eprints.lib.hokudai.ac.jp/>*****

420

421 **Acknowledgements**

422 We would like to thank the captain, crew and scientists on board the all research vessels
423 listed in Table S1 for their help with observations and sample collection. Thanks to Dr.
424 Y. N. Volkov and Mr. Scherbinin, the Far Eastern Regional Hydrometeorological

425 Research Institute, for their cooperation with the Japanese-Russian joint research
426 program. Thanks to Dr. Wakatsuchi, Ms Aiko Murayama and Dr. Toru Hirawake for
427 their helpful support for this study. Thanks to Dr. Hiroaki Saito and Dr. Yu Umezawa
428 for their nutrient measurement for the samples obtained during cruise KH-15-4. This
429 work was supported by the Grant-in-Aid for Scientific Research, the Ocean mixing
430 processes: OMIX project, (Grant Numbers JP15H05820, JP15H05817, 17H00775)
431 funded to JN, HOb, IY, the Arctic Challenge for Sustainability (ArCS) project, and the
432 Grant for Joint Research Program of the Institute of Low Temperature Science,
433 Hokkaido University.

434

435

436 **References**

437

- 438 1. J. H. Martin, S. E. Fitzwater, Iron deficiency limits phytoplankton growth in the
439 north-east pacific subarctic. *Nature* **331**, 341-343 (1988).
- 440 2. A. Tsuda et al., A mesoscale iron enrichment in the western subarctic Pacific
441 induces large centric diatom bloom. *Science* **300**, 958-961 (2003).
- 442 3. P. W. Boyd *et al.*, The decline and fate of an iron-induced subarctic phytoplankton
443 bloom. *Nature* **428**, 549-553 (2004).
- 444 4. T. Takahashi *et al.*, Global sea-air CO₂ flux based on climatological surface ocean
445 pCO₂, and seasonal biological and temperature effects. *Deep Sea Research part II*
446 **49**, 9-10, 1601-1622 (2002).
- 447 5. Y. Sakurai, An overview of Oyashio ecosystem. *Deep Sea Res. Part II* **54**,
448 2526-2542 (2008)
- 449 6. J. L. Sarmiento, N. Gruber, M. A. Brzezinski, J. P. Dunne, High-latitude controls of
450 thermocline nutrients and low latitude biological productivity. *Nature* **427**, 56-60
451 (2004).
- 452 7. W. S. Broecker, T.-H. Peng, *Tracers in the sea*, (Lamont-Doherty Geological
453 Observatory, Columbia University, 690 pp doi:10.2307/1309641 1982).
- 454 8. K. Matsumoto, R. M. Key, Natural radiocarbon distribution in the deep Ocean.
455 *Global Environmental Change in the Ocean and on Land*, Eds., M. Shiyomi et al.,
456 pp. 45-58. Terapub (2004).
- 457 9. K. Matsumoto, Radiocarbon-based circulation age of the world oceans. *J. Geophys.*
458 *Res.* **112**: C09004, doi: 10.1029/2007JC004095 (2007).
- 459 10. M. Kawabe, S. Fujio, Pacific Ocean circulation based on observation. *J. Oceanogr.*
460 **66**, 389-403 (2010).

- 461 11. J. Nishioka *et al.*, Intensive mixing along an island chain controls oceanic
462 biogeochemical cycles. *Global Biogeochem. Cycle* **27**, 920–929 (2013).
- 463 12. J. L. Sarmiento, N. Gruber, *Ocean Biogeochemical dynamics* (Princeton University
464 press, Princeton, New Jersey 2006).
- 465 13. I. Yasuda, The origin of the North Pacific Intermediate Water. *J. Geophys. Res.*
466 **102(C1)**, 893-909 (1997).
- 467 14. I. Yasuda *et al.*, Hydrographic structure and transport of the Oyashio south of
468 Hokkaido and the formation of North Pacific Intermediate Water. *J. Geophys. Res.*
469 **106(C4)**, 6931-6942 (2001).
- 470 15. L. D. Talley, An Okhotsk Sea Water anomaly: Implications for ventilation in the
471 North Pacific. *Deep Sea Res., Part I* **38**, S17 (1991).
- 472 16. P. W. Boyd, M. J. Ellwood, The biogeochemical cycle of iron in the ocean. *Nature*
473 *Geo.* **3**, 675-682 (2010).
- 474 17. T. M. Conway, J. G. Seth, Quantification of dissolved iron sources to the North
475 Atlantic Ocean. *Nature* **511**, 212–215 (2014).
- 476 18. A. Tagliabue *et al.*, Surface-water iron supplies in the Southern Ocean sustained by
477 deep winter mixing. *Nature Geo.* **7**, 314-320 (2014).
- 478 19. A. Taliabue, O. Aumont, L. Bopp, The impact of different external sources of iron
479 in the global carbon cycle. *Geophys. Res. Lett.* **41**, 920-926
480 doi:10.1002/2013GL059059, (2014).
- 481 20. A. Tagliabue *et al.*, The integral role of iron in ocean biogeochemistry. *Nature* **543**,
482 51-59 (2017).
- 483 21. J. A. Resing *et al.*, Basin-scale transport of hydrothermal dissolved metals across the
484 South Pacific Ocean. *Nature* **523**, 200-203, doi:10.1038/nature14577 (2015).
- 485 22. P. J. Lam *et al.*, Wintertime phytoplankton bloom in the subarctic Pacific supported
486 by continental margin iron. *Global Biogeochem. Cycle* **20**, GB1006,
487 doi:10.1029/2005GB002557 (2006).
- 488 23. P. J. Lam, J. K. B. Bishop, The continental margin is a key source of iron to the
489 HNLC North Pacific Ocean. *Geophys. Res. Lett.* **35**, L07608,
490 doi.org/10.1029/2008GL033294 (2008).
- 491 24. J. Nishioka *et al.*, Iron supply to the western subarctic Pacific: Importance of iron
492 export from the Sea of Okhotsk. *J. Geophys. Res.* **112**,
493 C10012 <https://doi.org/10.1029/2006JC004055> (2007).
- 494 25. J. Nishioka, H. Obata, Dissolved iron distribution in the western and central
495 subarctic Pacific: HNLC water formation and biogeochemical processes. *Limnol.*
496 *Oceanogr.* **62 (5)**, 2004-2022 (2017).

- 497 26. J. Nishioka *et al.*, Quantitative evaluation of iron transport processes in the Sea of
498 Okhotsk. *Prog. Oceanogr.* **126**, 180-193 (2014).
- 499 27. M. Schulz *et al.*, Atmospheric transport and deposition of mineral dust to the ocean:
500 implication for research need, *Environ. Sci. Technol.* **46**, (19), 10390–10404,
501 doi: 10.1021/es300073u (2012)
- 502 28. A. Ito, Z. Shi, Delivery of anthropogenic bioavailable iron from mineral dust and
503 combustion aerosols to the ocean, *Atmos. Chem. Phys.* **16**, 85-99,
504 doi.org/10.5194/acp-16-85-2016, (2016).
- 505 29. E. R. Sholkoviz, P. N. Sedwick, T. M. Church, A. R. Baker, C. F. Powell, Fractional
506 solubility of aerosol iron: Synthesis of a global-scale data set. *Geochem. Cosmochim.*
507 *Acta* **89**, 173-189, doi.org/10.1016/j.gca.2012.04.022 (2012).
- 508 30. W. K. Johnson, L. A. Millar, N. E. Sutherland, C. S. Wong, Iron transport by
509 mesoscale Haida eddies in the Gulf of Alaska, *Deep-Sea Res. II* **52**, 933-953 (2005).
- 510 31. S. Itoh *et al.*, Strong vertical mixing in the Urup Strait. *Geophys. Res. Lett.* **38**,
511 L16607, doi:10.1029/2011GL048507 (2011).
- 512 32. S. Itoh, I. Yasuda, T. Nakatsuka, J. Nishioka, Y. N. Volkov, Fine-and microstructure
513 observation in the Urup Strait, Kuril Islands, during August 2006. *J. Geophys. Res.*
514 **115**, C08004, doi:10.1029/2002JC005629 (2010).
- 515 33. M. Yagi, I. Yasuda, Deep intense vertical mixing in the Bussol' Strait. *Geophys. Res.*
516 *Lett* **39**, L01602, doi:10.1029/2011GL050349 (2012).
- 517 34. H. I. Palevsky, P. D. Quay, D. E. Lockwood, D. P. Nicholson, The annual cycle of
518 gross primary production, net community production, and export efficiency across
519 the North Pacific Ocean. *Global Biogeochem. Cycle*, 361-380,
520 doi:10.1002/2015GB005318 (2016).
- 521 35. M. Wakita *et al.*, Biological organic carbon export estimated from the annual
522 carbon budget observed in the surface waters of the western subarctic and
523 subtropical North Pacific Ocean from 2004 to 2013. *J. Oceanogr.* **72**, 665- 685,
524 10.1007/s10872-016-0379-8 (2016).
- 525 36. Y. Long, X-H. Zhou, X. Guo, The Oyashio Nutrient Stream and its Nutrient
526 Transport to the Mixed Water Region. *Geophys. Res. Lett.* **46**, 1513–1520,
527 doi.org/10.1029/2018GL081497 (2019).
- 528 37. T. Suga, M. Motoki, Y. Aoki, A. M. MacDonald, The North Pacific climatology of
529 winter mixed layer and mode waters. *J. Phys. Oceanogr.* **34**, 3-22 (2004).
- 530 38. S. Yasunaka, *et al.*, Mapping of sea surface nutrients in the North Pacific: Basin-
531 wide distribution and seasonal to interannual variability. *J. Geophys. Res.* **119**, 11
532 doi.org/10.1002/2014JC010318, (2014).

- 533 39. K. Suzuki *et al.*, Spatial variability in iron nutritional status of large diatoms in the
534 Sea of Okhotsk with special reference to the Amur River discharge, *Biogeosciences*
535 **11**, 2503–2517 doi: 10.5194/bg-11-2503-2014, (2014).
- 536 40. J. Nishioka, T. Ono, H. Saito, K. Sakaoka, T. Yoshimura, Oceanic iron supply
537 mechanisms which support the spring diatom bloom in the Oyashio region, western
538 subarctic Pacific. *J. Geophys. Res.* **112**, C10012, doi: 10.1029/2010JC006321
539 (2011).
- 540 41. World Ocean Atlas, National Centers for environmental information, NOAA,
541 <https://www.nodc.noaa.gov/OC5/woa18/2018>
- 542 42. K. I. Ohshima, S. Nihashi, K. Iwamoto, Global view of sea-ice production in
543 polynyas and its linkage to dense/bottom water formation. *Geosci. Lett.* **3**,
544 doi:10.1186/s40562-016-0045-4 (2016).
- 545 43. A. Marchetti, M. Maldonado, E. S. Lane, P. J. Harrison, Iron requirements of the
546 pennate diatom *Pseudo-nitzschia*: Comparison of oceanic (High-nitrate,
547 low-chlorophyll waters) and coastal species. *Limnol. Oceanogr.* **51**, 2092-2101,
548 doi:10.4319/10.2006.51.5.2092 (2006).
- 549 44. J. Nishioka, S. Takeda, C. S., W. K. Wong, Johnson Size-fractionated iron
550 concentrations in the northeast Pacific Ocean: distribution of soluble and small
551 colloidal iron. *Mar. Chem.* **74**, 157-179, doi.org/10.1016/S0304-4203(01)00013-5
552 (2001).
- 553 45. J. Nishioka et al., Size-fractionated iron distributions and iron-limitation processes
554 in the subarctic NW Pacific, *Geophys. Res. Lett.* **30(14)**,
555 doi:10.1029/2002GL016853 (2003).
- 556 46. H. Obata, H. Karatani, E. Nakayama, Automated determination of iron in seawater
557 by chelating resin concentration and chemiluminescence detection. *Anal. Chem.* **65**,
558 1524–1528 (1993).
- 559 47. K. S. Johnson et al., Developing standards for dissolved iron in seawater. *EOS* **88**,
560 131–132 (2007).
- 561 48. L. A. Anderson, J. L. Sarmiento, Redfield ratios of remineralization determined by
562 nutrient data analysis. *Global Biogeochem. Cycles* **8**, 65-80 (1994).
- 563 49. Y. Goto, I. Yasuda, M. Nagasawa, Turbulence estimation using fast-response
564 thermistors attached to a free-fall vertical microstructure profiler. *J. Atmos. Ocean*
565 *Tech.* **33**, 2065-2078. doi: 10.1175/JTECH-D-15-0220.1 (2016).
- 566 50. Y. Goto, I. Yasuda, M. Nagasawa, Comparison of turbulence intensity from
567 CTD-attached and free-fall microstructure profilers. *J. Atmos Ocean Tech.* **35**,
568 147-162. doi: 10.1175/JTECH-D-17-0069.1 (2018).

- 569 51. Y. Tanaka, I. Yasuda, H. Hasumi, H. Tatebe, and S. Osafune, 2012: Effects of the
570 18.6-year modulation of tidal mixing on the North Pacific bidecadal climate
571 variability in a coupled climate model, *Journal of Climate*, 25, 7625-7642 (2012).
572 52. R. Schlitzer, *Ocean Data View*. <http://odv.awi.de> (2018).
573

574 **Figure legends**

575

576 **Figure 1**

577 Comprehensive observation for investigating dissolved Fe in the North Pacific
578 conducted from 1998 to 2018. a) Observed stations for dataset and water current in the
579 subarctic Pacific, b) 3D dissolved Fe diagram in the North Pacific constructed by the
580 dataset (part of data is not included), GP02 in b) is line ID for the GEOTRACES
581 program, c) horizontal distribution of dissolved Fe at surface (5-10m), d) same as c) but
582 at isopycnal surface $26.8 \sigma_{\theta}$, e) same as c) but at isopycnal surface $27.5 \sigma_{\theta}$.

583

584

585 **Figure 2**

586 a) Horizontal distribution of dissolved oxygen at isopycnal surface $26.8 \sigma_{\theta}$, b) same as
587 a) but phosphate, c) vertical section profile of proportion of regenerated phosphate
588 along Line East Kamuchatka Current (EKC) in b), d) same as c) but along GP02 line in
589 b), e) same as c) but along Okh-155 in b), (※ Nutrient include the data referred from
590 JAMSTEC, MR04-04 cruise data,
591 <http://www.godac.jamstec.go.jp/darwin/cruise/mirai/mr04-04/j>). Black solid line in c, d,
592 e indicate isopycnal surface of $26.8, 27.0, 27.5 \sigma_{\theta}$, respectively.

593

594

595 **Figure 3**

596 a) horizontal distribution of nitrate+nitrite (N) concentration at surface (5-10m), b) same
597 as a) but isopycnal surface $26.8 \sigma_{\theta}$, Note that the color scale is different between Fig.3a
598 and Fig.3b. c) Vertical upward fluxes of N around the Kuril Islands chain, Aleutian
599 Islands chain, and the subarctic Pacific. d) Same as c) but for dissolved Fe. (※ Nutrient
600 for a) and b) include the data referred from JAMSTEC, MR04-04 cruise data,
601 <http://www.godac.jamstec.go.jp/darwin/cruise/mirai/mr04-04/j>)

602

603

604 **Figure 4**

605 The schematic draw of the circulation and intermediate water formation processes of
606 nutrients and dissolved Fe in the North Pacific, a) through the Bering Sea, b) through
607 the Okhotsk Sea, c) horizontal circulation. Regenerated nutrients and dissolved Fe in the
608 intermediate water are vertically supplied to surface layer by turbulent mixing around
609 the ICs and cycle between the intermediate and the surface layer. This nutrient

610 circulation in the intermediate water is coupled with intermediate dFe discharge from
611 the Okhotsk Sea. Then, nutrient and Fe are transported to eastward and to low latitude
612 by the NPIW, which influence to biological production at some hot spot in the North
613 Pacific.

614

615

616 **Figure 5**

617 a) Horizontal distributions of dissolved Fe to N ratio (nM/ μ M) at isopycnal surface 26.6
618 σ_θ in the North Pacific. b) Dissolved Fe vs nitrate+nitrite (N) plots, with Fe and N
619 demand ratio by dominated diatom (Black solid line used 3 μ mol Fe/mol C (ref 43) for
620 calculate Fe vs N), in Okhotsk sea shelf and the East Sakhalin, c) Same as b) but data
621 around the Kuril strait, d) Same as b) but data from 155°E to the west. e) Same as b) but
622 data from 155°E to the East, f) Same as b) but data around the Aleutian straits and in the
623 Bering Sea Basin. Color in b-f indicate water density (σ_θ). In the area b, c, d, the
624 Upper-intermediate water has high dissolved Fe concentration relative to N at a level to
625 relax & release iron limitation. In the area e and f, the Upper-intermediate water contain
626 not sufficient Fe for diatom growth. g) horizontal distributions of depth at isopycnal
627 surface 26.6 σ_θ , which depth is outcropped by winter mixing processes in the western
628 subarctic and the Oyashio-Kuroshio transition zone.

629

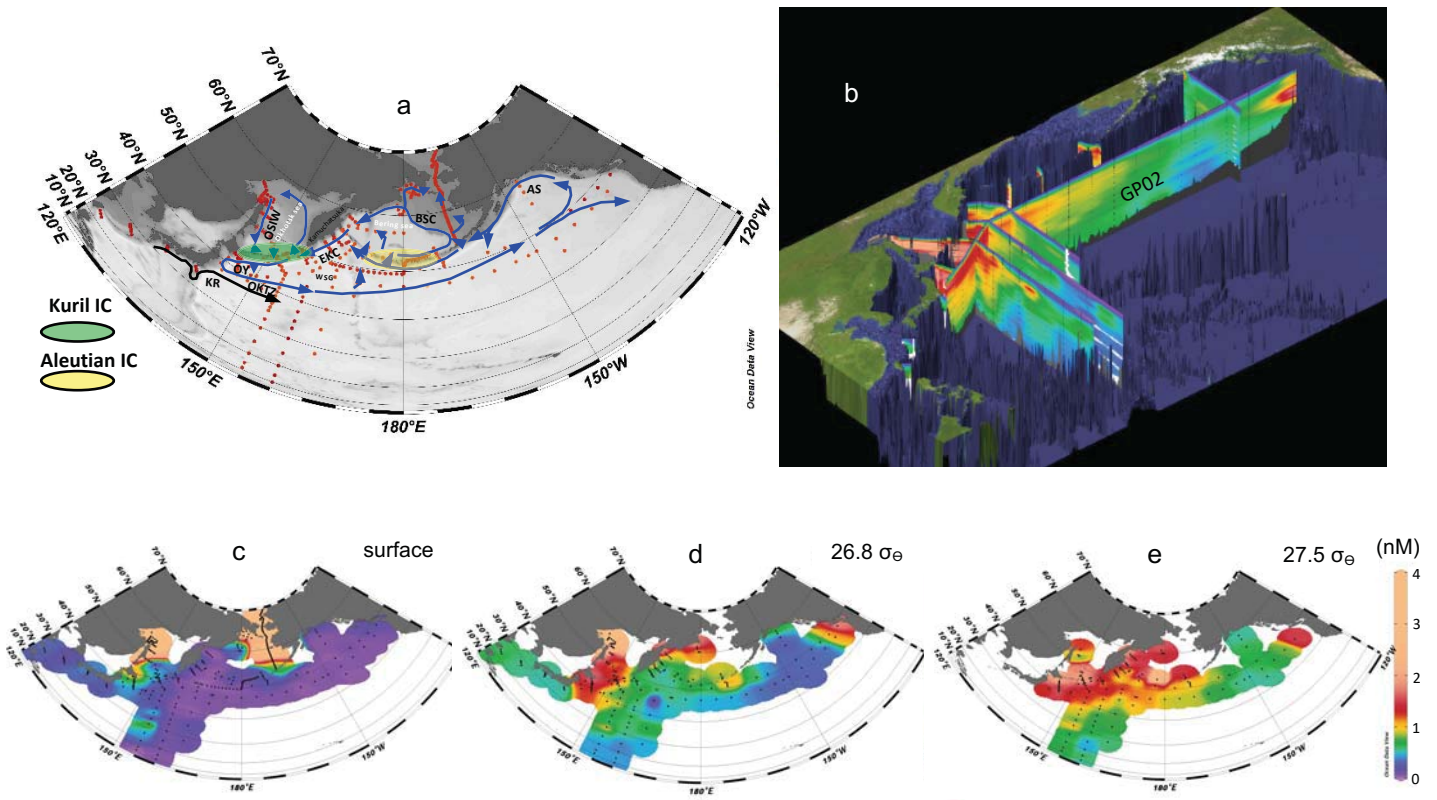


Figure 1

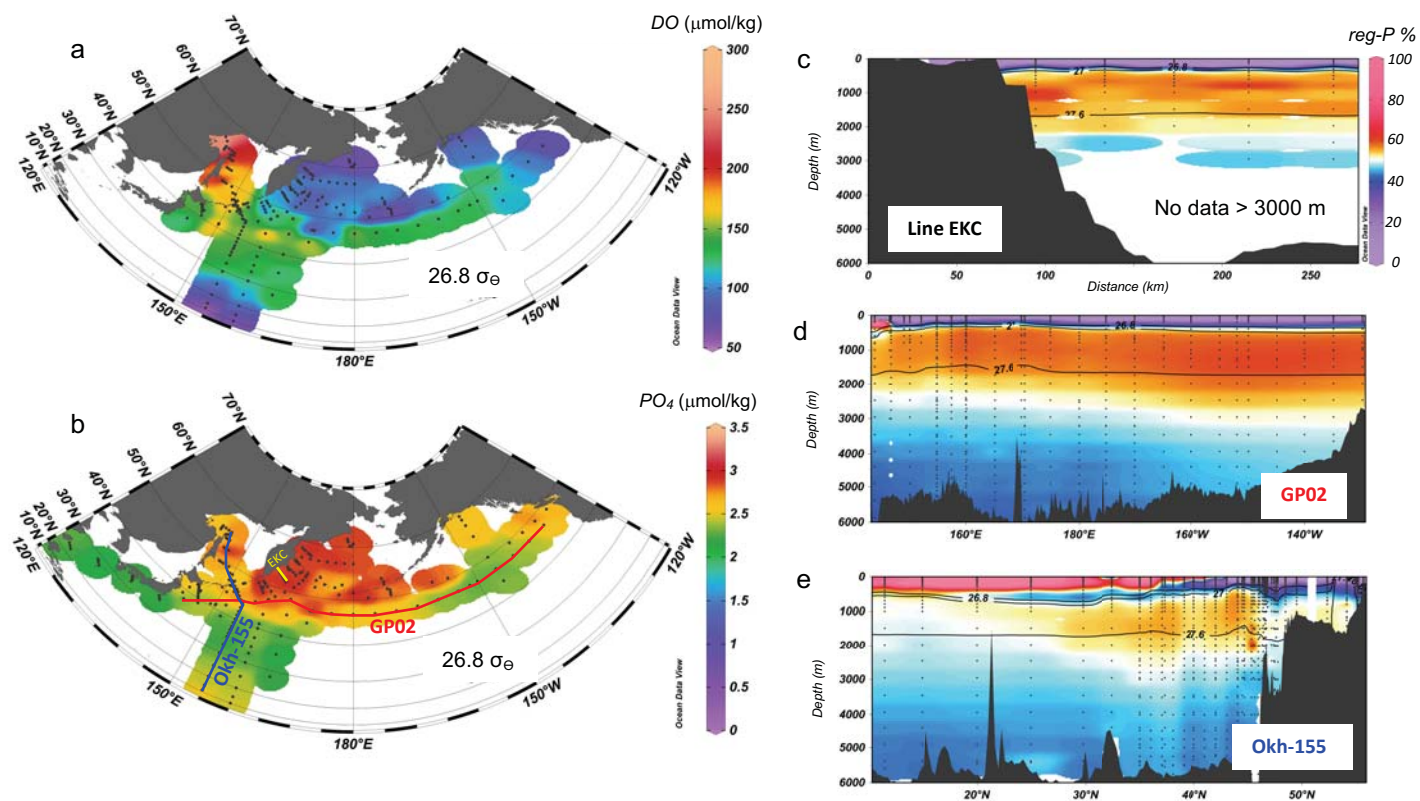


Figure 2

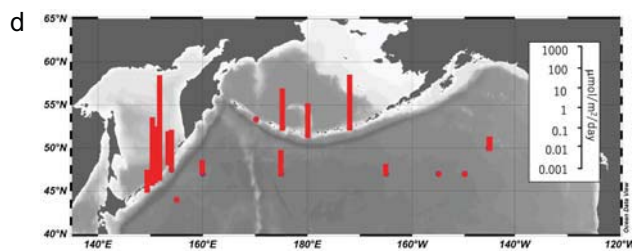
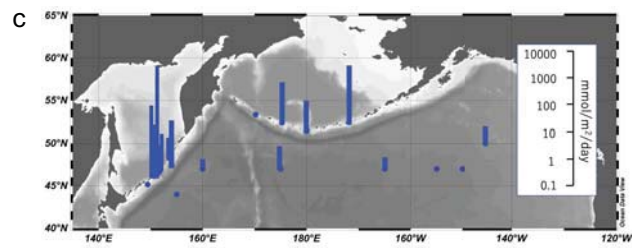
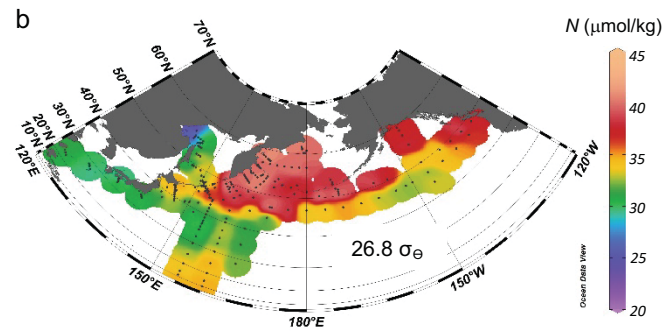
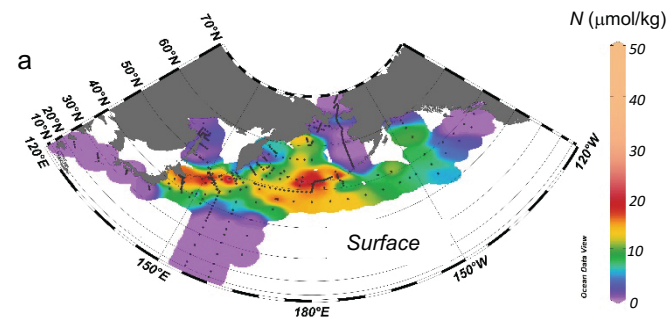


Figure 3

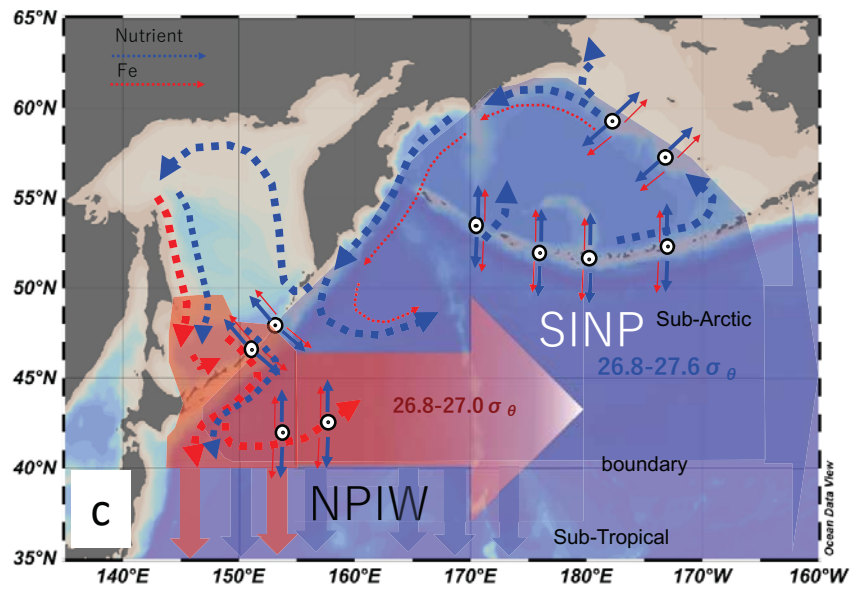
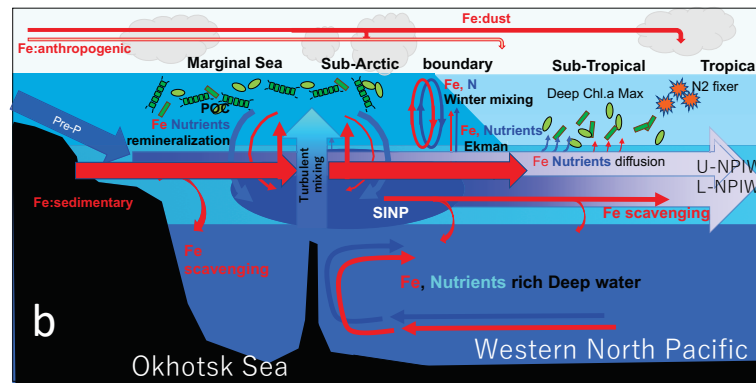
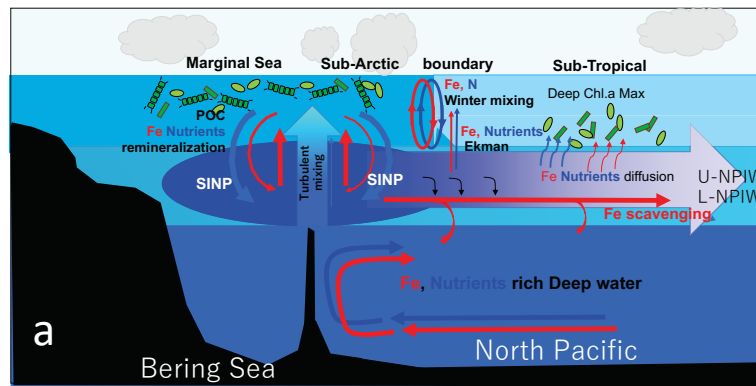


Figure 4

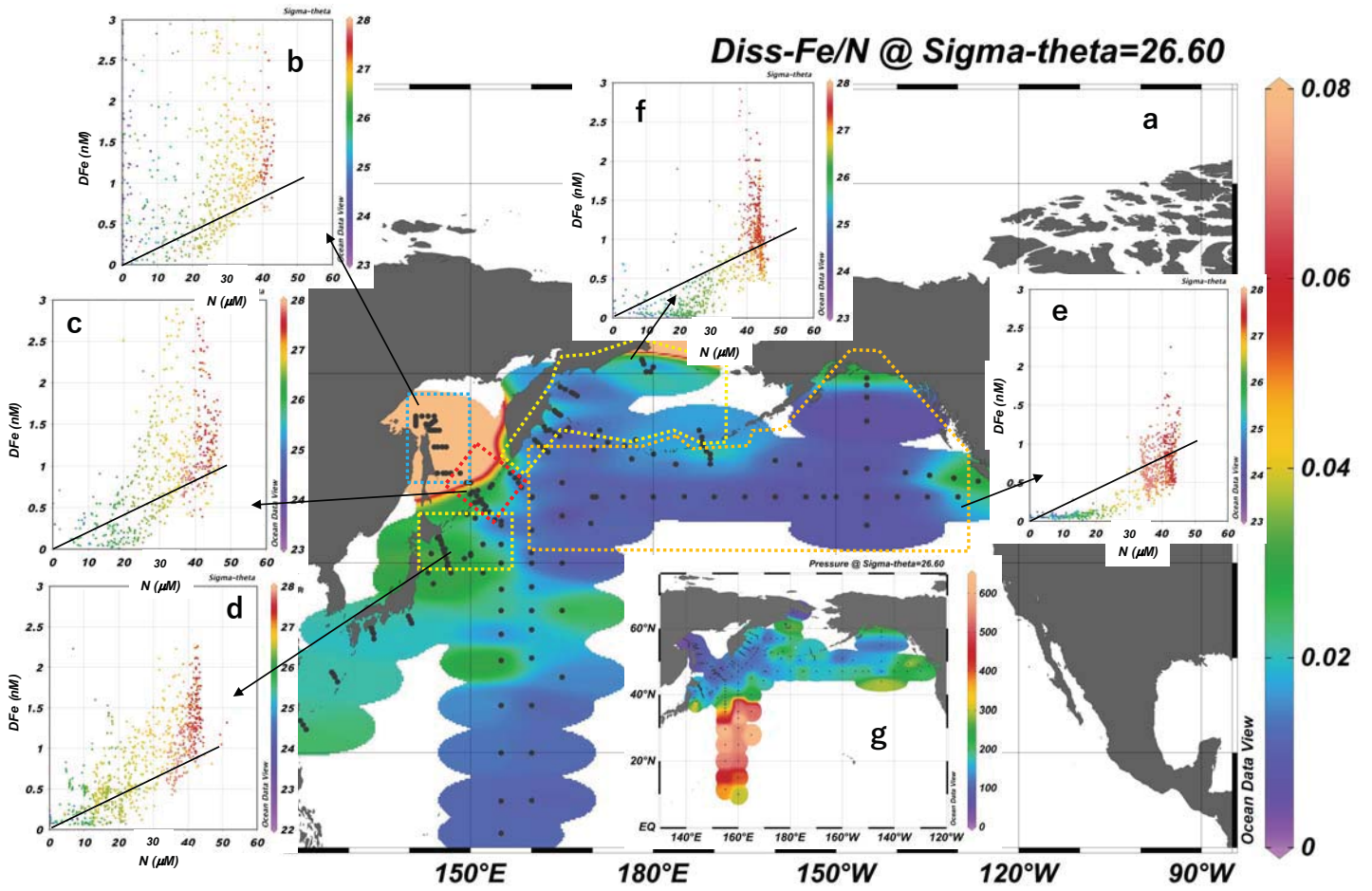


Figure 5